Elevation Performance of 1.25D and 1.5D Transducer Arrays

Douglas G. Wildes, *Member, IEEE*, Richard Y. Chiao, *Member, IEEE*, Chris M. W. Daft, *Member, IEEE*, K. W. Rigby, *Member, IEEE*, L. Scott Smith, *Member, IEEE*, and Kai E. Thomenius, *Member, IEEE*

***Abstract*—Present 1D phased array probes have outstanding lateral and axial resolution, but their elevation performance is determined by a fixed aperture focused at a fixed range. Multi-row array transducers can provide significantly improved elevation performance in return for "modest" increases in probe and system complexity. Time-domain simulations of elevation beam profiles are used to compare several types of multi-row probes.**

The elevation aperture of a 1.25D probe increases with range, but the elevation focusing of that aperture is static and determined principally by a mechanical lens with a fixed focus (or foci). 1.25D probes can provide substantially better near- and far-field slice thickness performance than 1D probes and require no additional system beamformer channels.

1.5D probes use additional beamformer channels to provide dynamic focusing and apodization in elevation. 1.5D probes can provide detail resolution comparable to, and contrast resolution substantially better than, 1.25D probes, particularly in the mid- and far-field.

Further increases in system channel count allow the use of 1.75D and 2D arrays for adaptive acoustics and two-dimensional beam steering. Significant improvements in clinical image quality can be expected as multi-row probes become increasingly available in the marketplace.

I. Introduction

The development of instruments for medical ultrasound has generated a steady improvement in axial and lateral resolution over the last 30 years. During this period transducers have developed from relatively low frequency, manually operated, single-element transducers to electronically steered linear arrays with more than 200 elements. Typical operating frequencies for general abdominal imaging applications have increased from 2.5 MHz or lower to 3.5 MHz or higher. This change has been achieved by the use of more sensitive pre-amplifiers, improvements in transducer technology, and better matching between the transducer elements and the transmit-receive electronics.

The common goal of all these changes has been the improvement in lateral and, to a lesser degree, axial resolution. It is, however, becoming increasingly difficult to improve upon these two parameters because the easily achievable modifications have already been implemented.

One aspect of system performance that has received relatively little attention in recent years is that of beamwidth in the plane perpendicular to the imaging plane, often referred to as the elevation beamwidth or slice thickness. Considerable attention was given to this issue in the late 1970's and early 1980's [1]–[5]. There are two main reasons slice thickness has received less attention than either lateral or axial resolution. First, changes in elevation beamwidth do not affect the display of a B-scan image as dramatically as do changes in lateral and axial resolution, because the improved direction is perpendicular to the plane of the display. Second, building transducer arrays with the required elevational properties has been difficult. The already small transducer elements must be further subdivided and independently controlled. Only with the recent development of more sophisticated electronics has the construction and control of the needed transducer arrays been successfully addressed. Moreover, due to reasons involving ease of fabrication, most of today's test phantoms involve cylindrical targets (e.g., wires or cylinders with varying diameters and backscatter strengths). These phantoms are especially insensitive to changes in elevational beamwidth which offer mainly improvements in contrast resolution and in the detectability of very small lesions.

To control the slice thickness, most current transducers use a fixed lens or curved transducer elements to create a fixed mechanical focus at a desired range. The f-numbers used with these designs are relatively high (e.g., $f/3$ to $f/6$ in elevation *vs.* $f/1$ to $f/2$ in azimuth). The goal is to have a reasonable depth of focus in the elevation direction.

The lack of attention to the elevation performance is slowly beginning to change. Three companies are advertising systems with electronically adjustable elevation focus. Rownd *et al.* [6] have developed spherical void phantoms with the specific goal of determining the ability of a scanner to detect small diameter, cyst-like targets. Similarly, Vilkomerson *et al.* [7] have proposed a new resolution metric with a similar goal: how well can an imager detect a small target in a region of uniform backscatter.

To address the elevation focusing issue, several different transducer schemes have been proposed [8]. In this paper, these schemes are referred to as 1D, 1.25D, 1.5D, 1.75D, and 2D arrays and are defined as follows:

- 1D: Elevation aperture is fixed, and focused at a fixed range.
- 1.25D: Elevation aperture is variable, but focusing remains static.
- 1.5D: Elevation aperture, shading, and focusing are dynamically variable, but symmetric about the centerline of the array.

Manuscript received July 1, 1996; accepted March 10, 1997.

The authors are with GE Corporate Research and Development, Schenectady, NY 12301 (e-mail: wildes@crd.ge.com).

1.75D: A 1.5D array without the symmetry constraint. Elements are large (several wavelengths) in elevation, so very little steering is possible.

2D: Elevation geometry and performance are comparable to azimuth, with full electronic apodization, focusing, and steering.

This paper illustrates the elevation beamforming capabilities of 1.25D and 1.5D arrays by exploring several of the tradeoffs which are inherent to the design of those arrays. A broadband three-dimensional simulator, described in Section II, is used to compute elevational beam profiles of specific transducer designs. A prototypic 1D linear array is defined in Section III. Section IV describes two alternative 1.25D extensions to the 1D design. Analytic approaches to optimizing the geometry and beamforming of a 1.5D array are explored in Section V; the performance of specific 1.5D designs is discussed in Section VI. Some of the features and issues associated with 1.75D and 2D arrays are reviewed in Section VII.

II. Modeling Acoustic Radiators

To investigate the properties of multi-row arrays, a computationally efficient three-dimensional simulator is required. Since typical imaging pulses are short, a time domain approach is appropriate. Harris [9], [10] has reviewed the classical methods for computing transient fields from baffled pistons. The method used here constructs the field from a plane radiator by convolution. The pressure $p(\mathbf{r},t)$ can be expressed as the convolution of a spatial impulse response $h(\mathbf{r},t)$ and the time derivative of the transducer response $\dot{E}(t)$:

$$p(\mathbf{r},t) \propto \dot{E}(t) \star h(\mathbf{r},t). \tag{1}$$

Piwakowski and Delannoy [11] give a method for efficiently computing $h(\mathbf{r},t)$:

$$h(\mathbf{r},t) = \frac{1}{4\pi}\int_{S'} \frac{v(x',y')\alpha(\theta)\delta[t - R/V_s - d(x',y')]}{R} dS'. \tag{2}$$

Here, $h(t)$ is in units of velocity potential divided by time [12]. The region of integration S' is the surface of the transducer. $v(x,y)$ is the normal component of the velocity of the surface of the transducer, $d(x,y)$ is the beamforming time delay at a given point, θ is the angle between the normal to dS' and the field point $\mathbf{r}$, $\alpha(\theta)$ is an inclination factor determined by the boundary condition, V_s is the speed of sound in tissue, and R is the distance from dS' to the field point $\mathbf{r}$.

In [11], a discrete representation of $h(\mathbf{r},t)$ is obtained which has a simple physical interpretation. Imagine the surface of the transducer divided into small areas ΔS_j. Each area emits a spherical, impulsive wave with propagation time

$$t_j = R_j + d_j \tag{3}$$

to the field point. (R_j and d_j are discretized versions of the variables R and $d(x,y)$ above.) The amplitude of the impulse received at the field point is proportional to the velocity of the elemental area v_j and to $1/R_j$. Piwakowski and Delannoy [11] show that, if the number of elemental areas is large enough, a band-limited approximation to the acoustic field can be obtained by summing the effect of each area in the radiator. In a numerical simulation, a vector represents the impulse response at the field point as a function of time. The time t_j is calculated for each elemental area on the transducer and specifies the element in the vector to which ΔS_j contributes. That element of the vector is incremented by $v_j\alpha/R_j$. This method of computing the integral has the virtues of speed and intuitive simplicity.

The dimensions of the transducer array are specified in $v(x,y)$; this matrix has zero entries for positions on the integration grid outside the transducer. A constant f-number can be maintained by changing $v(x,y)$ as a function of range. The effects of apodizing and shading are modeled with $v(x,y)$. The integration grid is substantially finer than the pitch of the transducer elements, which allows the angular response of each element to be included. The "inclination factor," a consequence of operating the high-impedance transducer into a comparatively low-impedance material (tissue), is modeled by $\alpha(\theta)$ in (2).

Steering and focusing information is encoded in the delay array $d(x,y)$. In the one-dimensional case, a physical lens in the elevation (y) direction is modeled by a fixed focus delay

$$\Delta t(y) = \frac{F_y}{V_s}\left[\sqrt{1 + \frac{y^2}{F_y^2}} - 1\right]. \tag{4}$$

This equation ignores refraction and the $1/\cos\theta$ dependence of the path length through the lens on the angle from each transducer source point to the field point. A comparison of (4) to a near-exact calculation of the lens effect shows, for the 1D probe in Fig. 1, that the time-delay error is less than the time quantization of our simulation for field points on the beam axis or in the mid and far field of the probe. Even in the near field, the error remains less than $\lambda/10$ for field points within the main lobe of the beam.

In a 1.5D, 1.75D, or 2D array, the elevation focal point F_y can be varied dynamically. The beam can also be steered in the y direction if there are enough elements (1.75D, 2D). In azimuth, the beam steering and focusing are done with the standard parabolic approximation [13]:

$$\Delta t(x) = \frac{1}{V_s}\left(-x\sin\theta + \frac{x^2}{2F_x}\cos^2\theta\right), \tag{5}$$

where F_x is the focal length. The effects of tap lengths in delay lines can be studied by quantizing $d(x,y)$.

Once the impulse response is calculated, the convolution in (1) is performed with FFTs. The result is a vector of pressure versus time for each field point. The maximum absolute value at each field point is used in the beam plots.

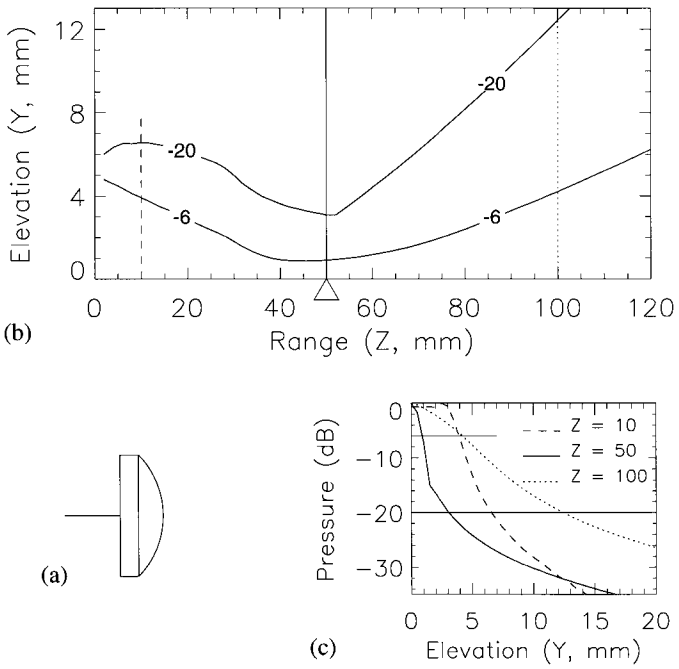

Fig. 1. Elevation performance of a 5 MHz, 1D linear array. The elevation aperture is 10 mm and the lens is focused at 50 mm (△). (a) Elevation cross-section of probe. (b) Contour plot of elevation cross-section of beam, normalized to 0 dB at each range. (c) Elevation beam profiles in near field (dashed line), at lens focus (solid line), and in far field (dotted line). Vertical lines on (b) show ranges of beam profiles in (c); horizontal lines on (c) show contours plotted in (b).

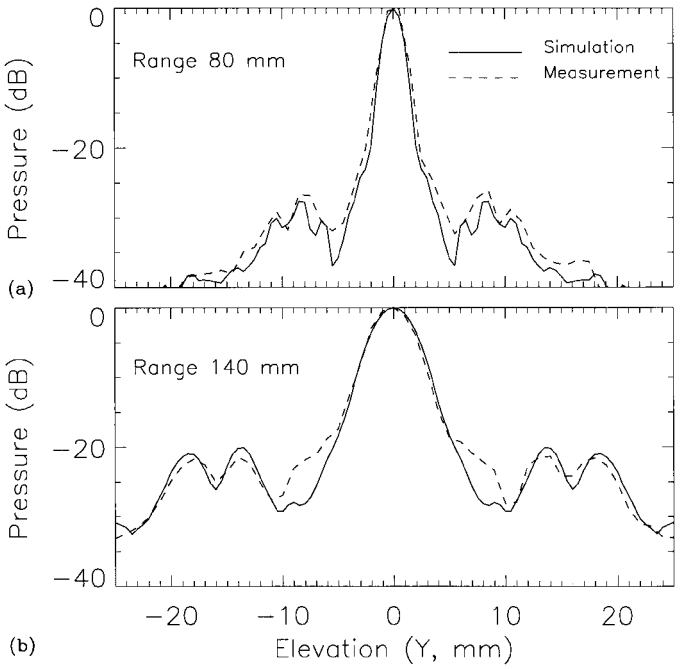

Fig. 2. Simulated (solid line) and measured (dashed line) beam profiles for a 3.75 MHz, 1.5D sector probe. The elevation aperture is 20 mm, divided into 5 rows, with a lens focused at 80 mm. Beam profiles shown are (a) at the lens focus and (b) in the far field.

For the simulations presented in this paper, the transducer array was sampled on a rectangular grid with pitch $\leq \lambda/4$, with a minimum of seven grid lines per transducer element in both elevation and azimuth. The impulse response at each field point was calculated with 5 nsec resolution. For the contour and beam profile plots, the acoustic field was sampled every 0.5 mm in elevation and every 2 mm in range. A typical simulation (Fig. 1) involved the calculation of time delays and amplitudes from about 10^5 points on the transducer to each of about 2500 field points and a 16K $\times$ 16K point convolution at each field point. In optimized C code on a Sun SPARC 20 workstation, this computation requires about 20 minutes.

To validate the simulation software, beam profiles of a 3.75 MHz 1.5D sector probe were measured [14]. Fig. 2 shows simulated versus measured elevation beam profiles at the lens focus (80 mm) and in the far field (140 mm). Since the simulations are one-way, one-way (receive only) measurements were made, using a small isotropic source (Specialty Engineering Associates, Milpitas, CA 95035) at the appropriate depth in the water tank. The level of agreement is sufficient to give good confidence in the operation of the simulation software. The structure of the sidelobes is largely due to the complex waveform from the isotropic source. Differences between the simulated and measured beam profiles may be due to an inexact match between the waveform used for the simulation and that achieved during the measurement or to differences between the time-delay beamformer of the simulator and the baseband beamformer of the measured imaging system. Other effects, such as refraction in the lens and quantization in the beamformers, are expected to be much smaller in magnitude.

III. 1D Array

As a reference case for this paper's exploration of multirow transducers, consider the prototypic 5 MHz 1D linear array transducer sketched in Fig. 1(a). In elevation, this probe has a 10 mm aperture and a 50 mm lens focus. In azimuth, the array has 128 elements at a pitch of 0.3 mm ($\approx \lambda$). A Gaussian impulse response with 70% bandwidth is assumed for ease of simulation.

A contour plot of the elevation beam profile of this array is shown in Fig. 1(b). This is a one-way (receive only) simulation of a beam directed perpendicular to the face of the transducer. The azimuthal aperture opens at $f/2$ and is dynamically focused at each range. The plot shows a slice through the center of the beam, perpendicular to the usual imaging plane. At each range, the maximum pressure in the beam profile is set to 0 dB, so the variation of sensitivity with range is normalized out. The contour plot therefore emphasizes the variation of the elevation beam width over the imaging range of the probe.

Fig. 1(c) shows elevation beam profiles at three ranges marked by the vertical lines in Fig. 1(b). The horizontal lines in Fig. 1(c) show the positions of the contour lines of Fig. 1(b). The −6 dB contour shows the main lobe width or detail resolution of a probe. The −20 dB contour is an

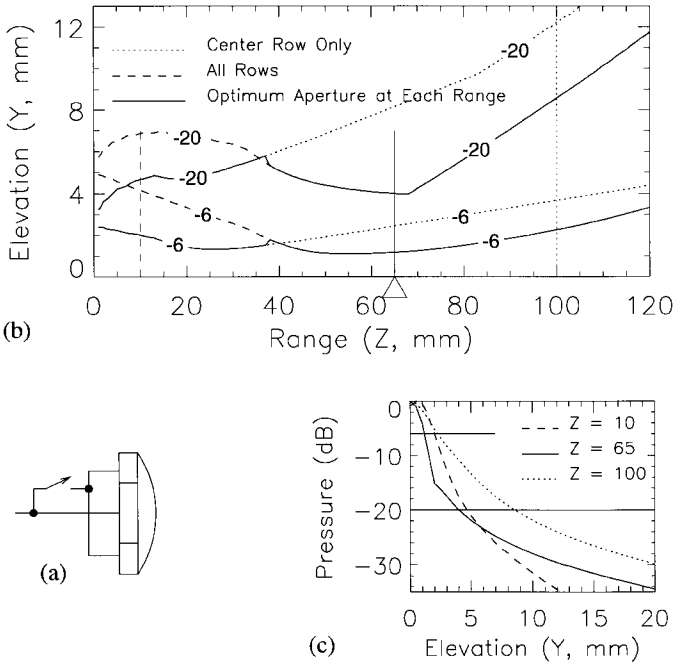

Fig. 3. A 1.25D array with a single-focus lens. The elevation aperture is 10 mm, divided into three rows, with a lens focused at 65 mm (△). (a) Elevation cross-section of probe, showing electrical connections to rows. (b) Contour plot of elevation cross-section of beam, normalized to 0 dB at each range. (c) Elevation beam profiles in near field, at lens focus, and in far field. Vertical lines on (b) show ranges of beam profiles in (c); horizontal lines on (c) show contours plotted in (b).

indicator of the width of the sidelobes and, therefore, of the contrast resolution of the probe.

The elevation performance of this simulated probe is typical of most commercial 1D array transducers. The focal length of the lens is chosen to give maximum contrast resolution near the imaging range of greatest importance for the intended application for the probe. The elevation aperture is a tradeoff between contrast resolution and sensitivity near the lens focus (improved by a larger aperture) and depth of field or contrast away from the focus (improved by a smaller aperture). An aperture between $f/3$ and $f/6$ is usually chosen. Such an aperture gives good slice thickness and contrast resolution near the lens focus, but rather poor performance in the near and far field.

IV. 1.25D Arrays

One approach to improving the near- and far-field elevation performance of a transducer is illustrated by the 1.25D array sketched in Fig. 3(a). The azimuthal properties of this array (and all subsequent 1.25D and 1.5D arrays) are identical to those of the 1D array described in Section III. The elevation of the transducer has been divided into three rows. The outer rows are electrically connected in parallel, and the signal leads from the elements in the combined outer rows are connected to the signal leads from the center row by an array of electronic switches (multiplexor). In practice, the outer rows are connected together within the probe head, whereas the multiplexor may be located within the probe head, at the console end of the probe cable, or within the system console itself. For the design simulated here, the combined area of the outer rows is equal to the area of the center row, so that their electrical impedances and acoustic sensitivities are equal.

Because changing the state of the mux switches generates noise, use of this probe typically requires two transmit-receive cycles per beam. With the mux switch open, the transmit delays are set to provide azimuthal focusing in the near field, and the near portion of the beam data is acquired. The mux switches are then closed, the transmit delays reconfigured, and the far field data is acquired. Data from the two zones are blended together in the imaging system, with care being taken to compensate for the change in sensitivity at the transition.

The near-field performance of this array is principally determined by the width of the center row. The focal length of the lens is in the far field for the center row ($d^2/4\lambda \approx 21$ mm for this array), so the lens has only a weak effect on the first zone. The far-field performance, however, is strongly affected by both the lens focus and the total elevation aperture. If the aperture is held constant, but the lens focal length is increased relative to that of the 1D transducer, the f-number and depth of field are increased and the far field of the 1.25D array is significantly improved, with a minimal effect on the near field. The contour plot in Fig. 3(b) and beam profiles in Fig. 3(c) show the performance with a 65 mm lens focus, 30% greater than the focal length of the 1D array in Fig. 1.

To further improve the elevation performance of the prototype transducer, while remaining within the constraints of 1.25D imaging (no dynamic focusing in elevation), consider the design in Fig. 4. This is a five-row array with a 12 mm elevation aperture and a multi-focus lens. As more rows are added to the array, the per-row width can be reduced to improve the near-field performance and the total elevation and lens focus may be increased to improve the far field.

The multifocus lens on this array, shown in Fig. 4(a), provides a delay function that is continuous across the elevation aperture but has a different curvature (focal length) for each row. Discontinuous delay functions are also possible, either by introducing discontinuities in the lens (which may cause diffraction artifacts) or by inserting static delay elements in the signal path between each row of elements and the mux [15], [16]. The advantage of a multifocus lens is that it substantially increases the depth of field, providing uniform resolution (−6 dB contour) and contrast (−20 dB contour) over essentially the entire imaging range of the probe. The disadvantage is that the sidelobes do not fall off quite as fast as those of a single-focus lens near its focal point. Compare the $Z = 65$ mm beam profile in Fig. 4(c) to that in Fig. 3(c).

Elevation contours for the example 1D and 1.25D designs are compared in Fig. 5(a). The 1.25D designs provide near-field and far-field performance (slice thickness ≈ contrast resolution) which is substantially better than con-

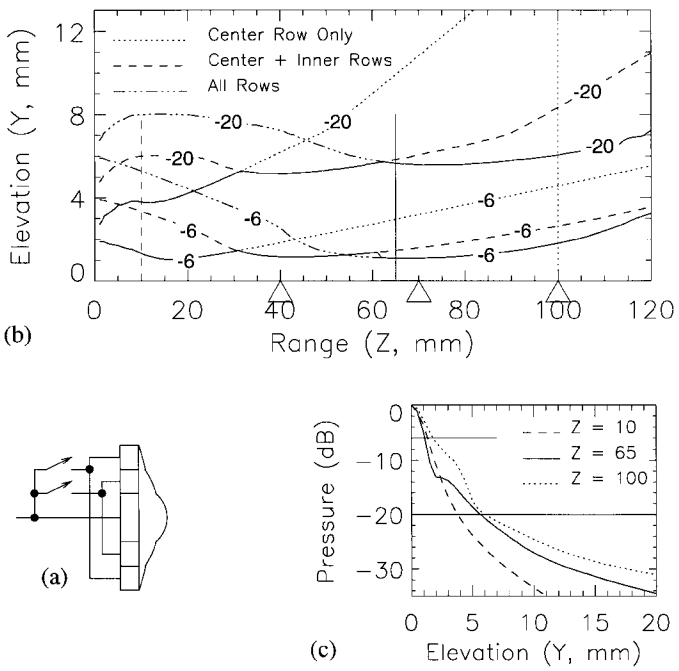

Fig. 4. A 1.25D array with a multi-focus lens. The elevation aperture is 12 mm, divided into five rows, with a lens focused (△) at 40 mm (center row), 70 mm (inner rows), and 100 mm (outer rows). (a) Elevation cross-section of probe. The lens profile is exaggerated. (b) Contour plot of beam, normalized to 0 dB at each range. The solid contours reflect use of the optimum aperture at each range. (c) Elevation beam profiles in near field, mid field, and far field.

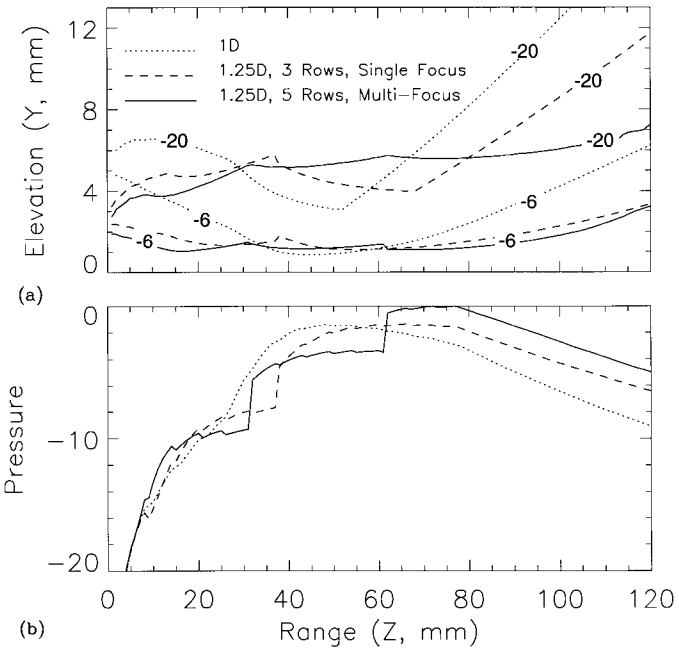

Fig. 5. Comparison of 1D and 1.25D array performance: The dotted lines are the 1D probe of Fig. 1, the dashed lines are the 3-row, single-focus 1.25D probe of Fig. 3, and the solid lines are the 5-row, multi-focus 1.25D probe of Fig. 4. All three probes are identical in azimuth: 128 elements, pitch 0.3 mm ($\approx \lambda$ at 5 MHz), dynamically focused, and dynamically apodized to maintain $f/2$. (a) Contour plot of beams, normalized to 0 dB at each range. (b) Sensitivity along the beam axis.

ventional 1D probes, and use no additional system beamformer channels. Although the system impact is minimal, the improved imaging performance comes at the cost of a significant increase in the complexity of the transducer pallet, cable assembly, and multiplexor. Fig. 5 shows that the increased elevation aperture and lens focal distance can contribute several dB to the probe's acoustic sensitivity in the far field; however, these gains may be offset by increased losses in the multiplexor and cable assembly.

V. "Optimal" 1.5D Elevation Geometry

1.5D arrays, which add dynamic elevation focusing to the features of 1.25D probes, offer the next level of improved elevation performance. To gain an appreciation for the number of parameters which must be specified in the design of a 1.5D probe, consider in more detail the elevation focusing described by (4): the time-delay error Δt at an elevation position y on a transducer for signals arriving from an on-axis field point at range R is:

$$V_s\,\Delta t(y,R) = \left(\sqrt{R^2+y^2}-R\right)-\left(\sqrt{F_{\text{lens}}^2+y^2}-F_{\text{lens}}\right) - \left[\left(\sqrt{R^2+y_{\text{eff}}^2}-R\right)-\left(\sqrt{F_{\text{lens}}^2+y_{\text{eff}}^2}-F_{\text{lens}}\right)\right] \tag{6}$$

where V_s is the speed of sound, the first term is the acoustic path length for an unfocused transducer, the second term is the elevation focusing provided by a fixed lens with focal distance F_{lens} (4), and the third term is dynamic elevation focusing by an electronic beamformer which treats the element as a point at elevation y_{eff}. For a 1.25D probe, with no dynamic focusing in elevation, $y_{\text{eff}} \equiv 0$ and the third term drops out. For simplicity, the constant terms are arranged to give zero delay error at y_{eff} and F_{lens}. Only the elevation axis is considered, so that the model is one-dimensional.

Expanding the square roots and keeping only the leading terms produces a simple parabolic model for all of the propagation and beamforming delays. With this approximation, the time-delay error becomes

$$2V_s\Delta t(y,R) = \frac{y^2}{R}-\frac{y^2}{F_{\text{lens}}}-y_{\text{eff}}^2\left(\frac{1}{R}-\frac{1}{F_{\text{lens}}}\right) \tag{7}$$

$$= \left(y^2-y_{\text{eff}}^2\right)\left(\frac{1}{R}-\frac{1}{F_{\text{lens}}}\right). \tag{8}$$

As a "simple" first case, consider a 1.5D probe with five rows and a single-focus lens. The array is symmetric about $y=0$, with the outer limits of the rows at $\pm y_1$, $\pm y_2$, and $\pm y_3$ (Fig. 6). The center row extends across $y=0$ and the outer rows are electrically connected in pairs across $y=0$, so that the elevation beamforming is also symmetric [Fig. 7(a)]. The effective y positions of the paired rows for beamforming are y_1^{eff}, y_2^{eff}, and y_3^{eff}.

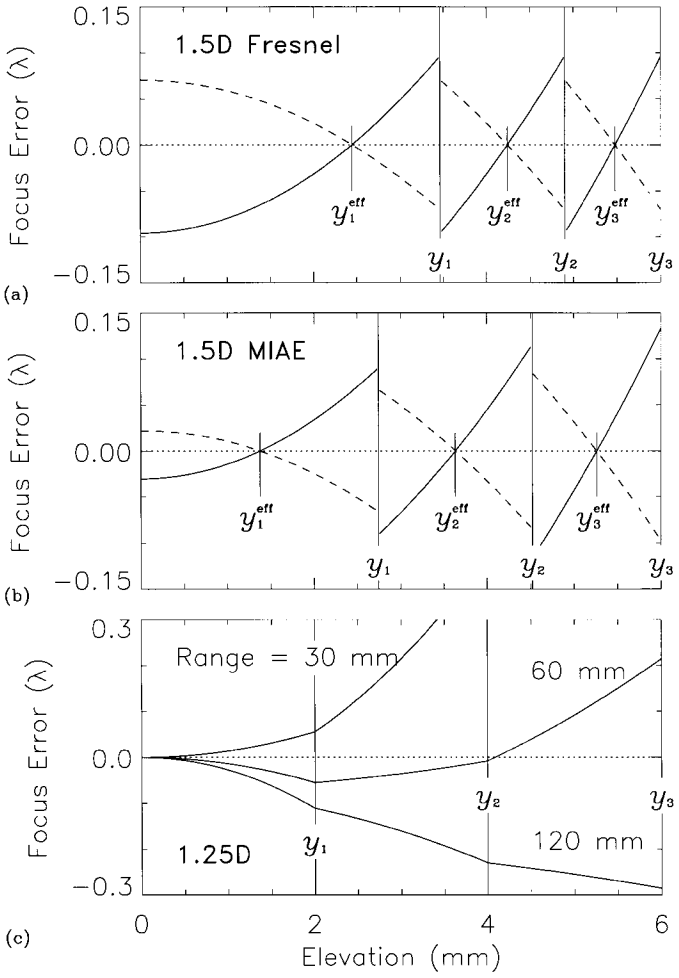

Fig. 6. Focus error (in wavelengths) across the elevation aperture at representative ranges for different 1.5D and 1.25D elevation geometries. (a) 1.5D Fresnel array with row widths and y^{eff} (for electronic focusing) determined by (12) and (13). The lens focus is at 65 mm; focus errors are plotted at 40 mm (solid lines) and 120 mm (dashed lines). The maximum absolute time-delay error is range-dependent and occurs at the array center and the row boundaries. As the focal distance varies, the focus error curve is scaled, but its shape does not change. (b) 1.5D probe with Minimum Integrated Absolute time-delay Error (MIAE). Row widths and y^{eff} are determined by (17) and (18). The lens focus is at 65 mm; focus errors are plotted at 40 mm (solid lines) and 120 mm (dashed lines). (c) 1.25D probe with equal-area rows and a multifocus lens (Fig. 4). The focus error is plotted at the turn-on range for the inner rows (30 mm), at the turn-on of the outer rows (60 mm), and in the far field. The shape of the focus error curve varies with range.

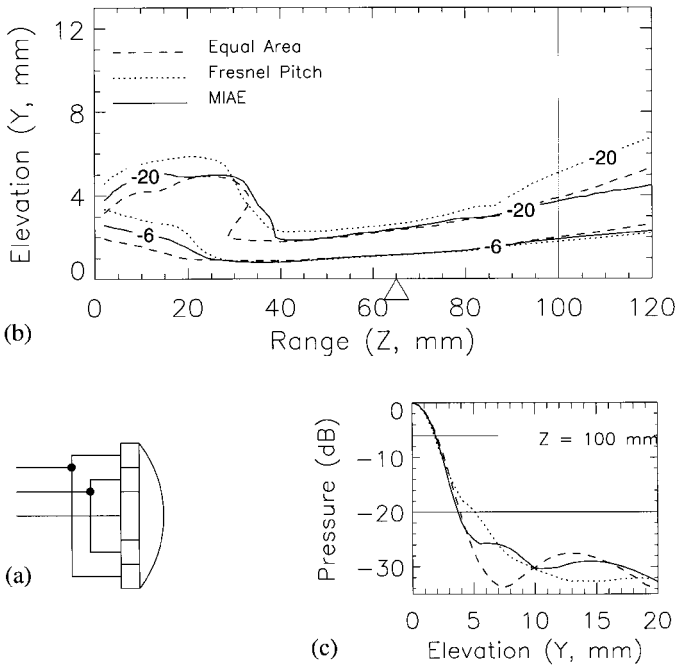

Fig. 7. Comparison of 1.5D arrays with equal-area rows (dashed line), Fresnel row pitch (dotted line), and Minimum Integrated Absolute time-delay Error row pitch (MIAE, solid line). Each probe has a 12 mm elevation aperture divided into five rows and a lens focused at 65 mm (△). (a) Elevation cross-section of probe (equal area), showing electrical connections to rows. (b) Contour plot of beams, normalized to 0 dB at each range. (c) Elevation beam profiles in the far field.

A criterion for minimizing the time-delay errors can be used to determine the relative row widths and the effective y positions for beamforming. The total elevation aperture must be established independently (otherwise the minimum error solution is an array of zero width). Along with the probe and beamforming geometry, the elevation apodization must also be specified. In practice, with the exception of the very near field, best 1.5D performance is obtained with all rows active at all ranges. Dynamic shading in elevation plays a critical role in determining the beam profile, but it is not included in the present time-delay error analysis. As a result, the following solutions are most relevant near and beyond the lens focus, where the aperture is wide open and the shading is relatively flat.

One approach to optimizing the array is to minimize the maximum absolute time-delay error across the aperture. This leads to a solution with equal absolute error at the inner and outer edge of each row:

$$|\Delta t(y=0,R)| = |\Delta t(y_1,R)| = \ldots = |\Delta t(y_{\text{N}},R)| \tag{9}$$

With a single-focus lens, the dependence of (8) on R and F_{lens} factors out and (9) reduces to:

$$\begin{aligned} &\left|0-(y_1^{\text{eff}})^2\right| = \left|y_1^2-(y_1^{\text{eff}})^2\right| \\ =\ &\left|y_1^2-(y_2^{\text{eff}})^2\right| = \left|y_2^2-(y_2^{\text{eff}})^2\right| \\ =\ &\left|y_2^2-(y_3^{\text{eff}})^2\right| = \left|y_3^2-(y_3^{\text{eff}})^2\right|, \end{aligned} \tag{10}$$

which may be quickly solved:

$$\begin{aligned} (y_{\text{i}}^{\text{eff}})^2 &= (1/2)(y_{\text{i}-1}^2+y_{\text{i}}^2) \\ y_{\text{i}}^2-y_{\text{i}-1}^2 &= \text{constant} \end{aligned} \tag{11}$$

with $y_0 \equiv 0$. This is a version of the classic Fresnel lens [13]. Numerically, for a five-row array,

$$(y_1,\, y_2) \approx (0.577,\, 0.817)y_3 \tag{12}$$

$$(y_1^{\text{eff}},\, y_2^{\text{eff}},\, y_3^{\text{eff}}) \approx (0.408,\, 0.707,\, 0.913)y_3. \tag{13}$$

A plot of the time-delay error across the elevation aperture for a probe of this design is shown in Fig. 6(a). Note that y_{eff} of the center row is nonzero. This can be made zero, by adding a constant time-delay error across the array, which is, of course, irrelevant.

An alternate approach to optimizing the design of a 1.5D array is to minimize some average of the time-delay error over the entire aperture, rather than just the worst-case error at a few points. Consider, for instance, the absolute value of the time-delay error integrated across the array:

$$I(y_1, y_2, y_1^{\text{eff}}, y_2^{\text{eff}}, y_3^{\text{eff}}) = \int_0^{y_1} |\Delta t_1| dy + \int_{y_1}^{y_2} |\Delta t_2| dy + \int_{y_2}^{y_3} |\Delta t_3| dy, \quad (14)$$

where $\Delta t_i(y, y_{\text{i}}^{\text{eff}})$ is the time-delay error across the ith row, and the factor of two due to symmetry has been omitted. The integrated error I is minimized by imposing

$$\begin{aligned} \partial I/\partial y_{\text{i}} &= 0, \qquad i = 1, 2 \\ \partial I/\partial y_{\text{i}}^{\text{eff}} &= 0, \qquad i = 1, 2, 3, \end{aligned} \quad (15)$$

which leads to

$$\begin{aligned} y_{\text{i}}^{\text{eff}} &= (1/2)(y_{\text{i}-1} + y_{\text{i}}) \\ y_2/y_1 &= \sqrt{7} - 1 \\ y_3/y_1 &= 1 - \sqrt{7} + \sqrt{57 - 16\sqrt{7}}, \end{aligned} \quad (16)$$

with $y_0 \equiv 0$. Numerically,

$$(y_1, y_2) \approx (0.458, 0.754) y_3 \quad (17)$$

$$(y_1^{\text{eff}}, y_2^{\text{eff}}, y_3^{\text{eff}}) \approx (0.229, 0.606, 0.877) y_3. \quad (18)$$

The time-delay error across the elevation for this design is shown in Fig. 6(b). Relative to the Fresnel design in Fig. 6(a), the focus error in the center of the array is substantially reduced and the error on the outer rows is only modestly increased.

Minimizing the integrated squared error leads to a slightly different choice of row widths and effective positions, but the resulting beamprofiles are similar.

As a second test case for the analytic optimization of a multi-row probe design, consider a 1.25D probe with a multifocus lens. Dynamic focusing and shading in elevation are not available, and the elevation performance of the probe is determined by the row widths, turn-on ranges, and lens foci. A range-independent optimization of (8) in the far field no longer makes sense; a global optimization which balances the performance of the one-row, three-row, and five-row apertures is needed.

The authors have tried several different analytic optimization strategies with little success. Minimizing the integral of the absolute value of the time-delay error is analytically intractable. Minimizing the worst-case absolute time-delay error at the turn-on range for each row and at some arbitrary point in the far field is feasible, but leads to designs with only mediocre elevation performance. Neither approach provides enough constraints to determine all the free parameters in the design. In the end, equal-area rows were selected for uniformity of element impedance and the lens foci and turn-on ranges were determined by trial and error. The resulting transducer design was described in Section IV; its elevation performance is shown in Fig. 4, and the time-delay error across its aperture is shown in Fig. 6(c).

VI. 1.5D Arrays

In order to support dynamic elevation focusing, 1.5D arrays require many more beamforming channels and connections than 1.25D arrays. Elevational beam control for 1.25D arrays is accomplished only with a lens and multiplexor. All elements within each elevational column of a 1.25D array are connected to the same beamforming channel and share the same electronic time delay and shading. In contrast, 1.5D arrays use dynamic focusing and shading to control the elevational beam. With elevational symmetry (no steering), this requires an independent beamforming channel for each pair of elevational elements, as illustrated in Fig. 7(a).

The design of the row widths and lens should optimize the round-trip beam generated with dynamic focusing and shading over all ranges of interest. In azimuth, an element is well approximated by a point source at the center of the element for purposes of computing the beamforming delay; however, the proper choice of beamforming delay for a wide elevational element is less clear, since there is a range of distances between that element and any single point in space.

The distinction between a simple and compound lens is less important for 1.5D than 1.25D. In a 1.25D array the lens is the only focusing mechanism and having a compound lens is crucial for maintaining good detail and contrast resolution over an extended range. In a 1.5D array the electronic focusing and apodization are sufficiently effective that a compound lens provides little advantage over a simple lens. The lens focus should be near the center of the range of interest. For the prototypic 5 MHz probe with a range of interest from 5 to 120 mm, a lens focus of 65 mm is effective.

Three different strategies for selecting the row widths of a 1.5D probe are compared in Fig. 7. The design with equal-area rows (dashed line) provides uniform element impedance and sensitivity. The Fresnel design (12) (dotted line) minimizes the maximum delay error across the aperture. The Minimum Integrated Absolute time-delay Error (MIAE) design (17) (solid line) is the result of the optimization strategy described in Section V.

In the far field, as shown by the beam profiles in Fig. 7(c), the MIAE optimization strategy pays off. The MIAE probe has low, relatively uniform sidelobes, avoiding both the -18 dB shoulder of the Fresnel beam profile and the -27 dB grating lobe of the equal area probe. In the near field, the elevation performance is determined by

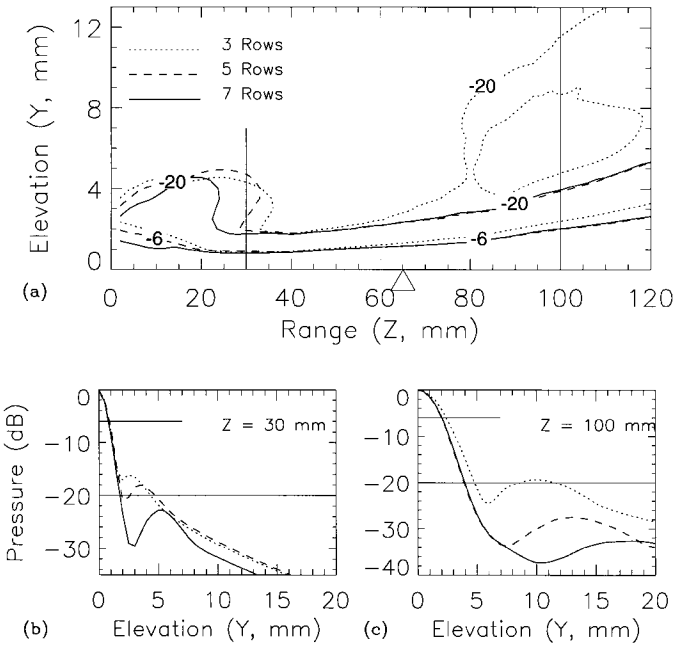

Fig. 8. Comparison of 1.5D arrays with three (dotted line), five (dashed line), and seven (solid line) rows. Each probe has a 12 mm elevation aperture divided into rows of equal area and a lens focused at 65 mm (△). (a) Contour plot of beams, normalized to 0 dB at each range. (b) Elevation beam profiles in near field. (c) Elevation beam profiles in far field.

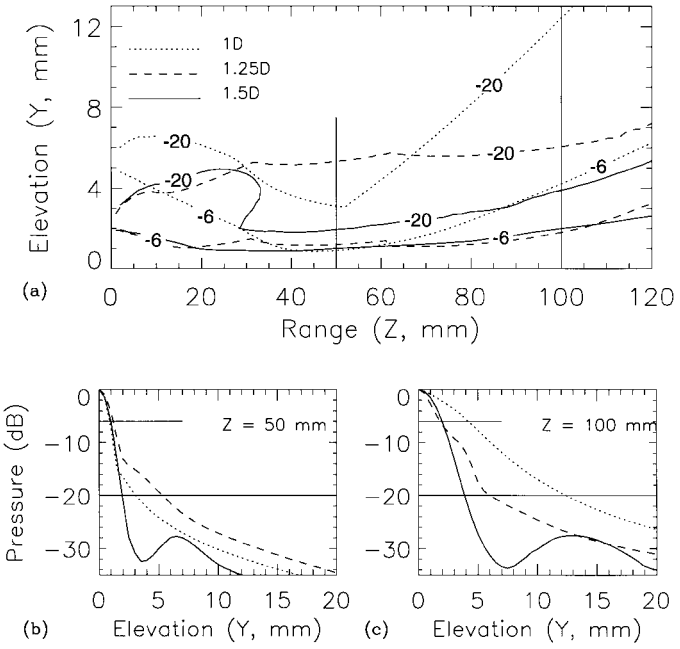

Fig. 9. Comparison of 1D, 1.25D, and 1.5D array performance: The dotted lines are the 1D probe of Fig. 1, the dashed lines are the five-row, multifocus 1.25D probe of Fig. 4, and the solid lines are the five-row, equal-pitch 1.5D probe of Figs. 7 and 8. (a) Contour plot of beams, normalized to 0 dB at each range. (b) Elevation beam profiles near the lens foci. (c) Elevation beam profiles in the far field.

the width of the center row and the equal area design will have an advantage. The contour plot of Fig. 7(b) compares the three design strategies over the entire imaging range of the probe. The near field performance of the equal area design clearly outweighs the relatively subtle advantages of the MIAE design in the far field.

Fig. 8 shows the effect of changing the number of rows while holding the total aperture constant. Because the total apertures are the same, all three designs have comparable detail resolution (−6 dB contours), except in the very near field, where the elevation performance is determined by the size of the center row. The principal effect of the number of rows and the row widths is on the contrast resolution, as indicated by the −20 dB contours and by the sidelobe levels in the beam profiles. The seven-row array has sidelobes 7 to 12 dB lower than the three-row probe, and twice the depth of field. The five-row probe is only marginally better than the three-row in the near field, but approaches the performance of the seven-row in the far field.

Elevation contours and beam profiles of representative 1D, 1.25D, and 1.5D arrays are compared in Fig. 9. The 1.25D and 1.5D probes provide similar, relatively uniform detail resolution (−6 dB contours) over the entire imaging range. The 1.5D probe offers substantially superior contrast resolution (−20 dB contours and sidelobes in beam profiles).

The simulations above assume 128 channels for every row of the array. In practice, the allocation of channels to rows is an important design choice given the limited number of beamformer channels available. To preserve azimuthal performance, it is important that the active azimuthal aperture and element pitch of a 1.5D probe be comparable to those of the competitive 1D probes. Use of the full aperture of a three- or five-row 1.5D probe could therefore require two or three times the number of beamformer channels as are used by a comparable 1D probe.

Fortunately, the situation is not quite this bad. An elliptical active aperture reduces the number of channels used by the outer rows and produces a beam profile which is superior to the beam profile of a rectangular aperture [14]. In addition, synthetic aperture techniques and multiple transmit-receive cycles may be used to obtain 256- or 512-channel performance from a 128-channel imager. Fully optimizing the performance of a 1.5D probe involves delicate tradeoffs between the effective channel count, the number of transmit focal zones along each beam, and the frame rate of the resulting image. The optimum transducer design may be one which supports several different modes of operation, for B-mode versus color-flow imaging and for low-tissue-motion radiology studies versus more rapid-movement vascular, obstetrical, and cardiac imaging.

VII. 1.75D and 2D Arrays

For completeness, some of the performance features and problems expected from 1.75D and 2D probes are outlined here. As mentioned in the introduction, release from the elevation symmetry constraint is the major feature which

separates 1.75D and 2D arrays from 1D, 1.25D, and 1.5D arrays. With independent control of the beamforming time delays for all elements in the aperture, 2D beam steering and other types of dynamic beam shaping become possible.

With 1.75D transducers, where the element dimensions and row pitch in elevation are large compared to an acoustic wavelength, elevation beam steering is constrained by the small acceptance angle of the elements and by grating lobes close to the main beam. When the beam is directed straight ahead, the grating lobes of a dense, equal-pitch array coincide with nulls of the single-element diffraction pattern and have little power. As the beam is steered in elevation, the main beam loses power as it moves away from the peak of the element directivity function, while a grating lobe gains power as it moves toward the peak. Elevation steering of 1.75D arrays is, therefore, limited to angles within a few degrees of a plane normal to the face of the array.

While not sufficient for full 3D imaging, this limited steering capability may be very useful for vector flow applications and for small deflections of the imaging plane to measure the 3D extent of small cysts, vessels, and other structures in the body. In addition, providing an independent beamforming channel for each transducer element allows one to compensate for inhomogeneous propagation velocities in the body (or nonuniformities in the imaging system or transducer). Called phase aberration correction or adaptive acoustics, such imaging approaches offer the promise of substantial improvement in image quality and are an active research area [17]–[20].

As the number of elevation rows in the transducer increases and the size of the elements decreases, the importance of a fixed physical lens decreases. When the elements are large in elevation, the time delay variation across a single element is still so large that a lens is required. As the element size decreases, the lens can be abandoned in favor of fully electronic beamforming.

Only when the array pitch in both elevational and azimuthal directions becomes comparable to a half wavelength (*i.e.*, true 2D arrays) are the benefits of full 3D beamforming realized [21]. With this small element size, beamsteering at substantial angles in elevation (>20 degrees) is now possible. Moreover, oblique imaging planes unconstrained by the axes of the probe can be selected under fast electronic control rather than by comparatively slow manual repositioning of the probe. Again, there are two realms of interest, dense and sparse, based on element coverage of the aperture. In a fully dense array with the order of 100 elements in both azimuth and elevation [2], the total number of elements (∼10,000) is significantly larger than anything currently in use. Sparse arrays, however, have been used by several groups [22]–[24] to study various aspects of electronically controlled 3D ultrasound imaging. Although the spacing between individual elements is on average larger than about a half wavelength, there are enough instances within the array where the sampling is at high spatial frequencies to suppress sidelobes to a respectable level. Specialized signal processing algorithms designed explicitly for such sparse array structures provide satisfactory beamprofiles over a wide range of azimuthal and elevational angles [25]–[27].

Both 1.75D and 2D arrays present substantial challenges to the system designer. As the array elements become smaller, the fabrication difficulties associated with making electrical connections to the individual elements increase rapidly. The increasing number of cables required to connect the transducer elements to the rest of the system causes problems of size, weight, and cable management. The impedance mismatch between the element and the cable rapidly worsens as the element size decreases [23]. Moreover, the effective signal-to-noise ratio drops precipitously. Both of these effects can be reduced by integrating some beamformer electronics with the transducer; however, this kind of integration is likely to be most effective when used with nontraditional beamformer architectures.

The large number of elements leads to other difficulties. As the number of elements in the array increases, either the number of independent electronic channels in the beamformer must also increase or some multiplexing scheme must be used to select subsets of elements for connection to a smaller number of electronic beamforming channels. These two choices lead to a large increase in system cost or a significant reduction in image acquisition frame rate, respectively. Since neither of these options is attractive, there is considerable opportunity for creative engineering, either as an optimized tradeoff among the various constraints or as a paradigm shift to an entirely new approach circumventing the current difficulties.

VIII. Conclusions

Elevation beam profiles of 1D and multi-row transducer arrays were calculated using a three-dimensional time-domain simulator. Present 1D phased array probes have outstanding lateral and axial resolution, but their elevation performance is determined by a fixed aperture focused at a fixed range. Several types of multi-row array transducers, which provide significantly improved elevation performance in return for "modest" increases in probe and system complexity, were reviewed.

The elevation aperture of a 1.25D probe increases with range, but the elevation focusing of that aperture is static and determined principally by a mechanical lens with a fixed focus (or foci). 1.25D probes can provide substantially better near- and far-field slice thickness performance than 1D probes, and require no additional system beamformer channels.

1.5D probes use additional beamformer channels (at least twice as many) to provide dynamic focusing and apodization in elevation. 1.5D probes can provide detail resolution comparable to, and contrast resolution substantially better than, 1.25D probes, particularly in the mid- and far-field.

Further increases in system channel count will allow the use of 1.75D and 2D arrays for adaptive acoustics and two-

dimensional beam steering. Several academic groups and many medical ultrasound companies are actively developing the probe and system technology necessary for multi-row transducer arrays. New breakthroughs in image quality can be expected as the results of their efforts become available in the marketplace.

Acknowledgments

The authors would like to thank their colleagues at GE CRD and GE Medical Systems, including Motoyoshi Ando, Walt Berninger, Ajay Bhave, Ed Bielawa, Elizabeth Burke, Carl Chalek, Stanley Chim, John David, Ray DeLaRosa, Tom Deitrich, Len Douglas, Evan Downey, Lonnie Edelheit, Lisa Fancovic, Mike Fazzone, Gregg Frey, Takeuki Goto, Anne Hall, Dave Hanchar, Mike Harsh, Bill Hatfield, Bill Hennessy, Omar Ishrak, Amanda Jeffries, Brady Jones, Jack Keres, John Kese, Bill Kornrumpf, Kris LaConte, Aminah Lawery, Don Lester, Bill Leue, Bob Lewandowski, Greg Lillegard, Ric Lisowski, Xuan-Ming Lu, Brian McEathron, Dan Miller, Steve Miller, Larry Mo, Atsushi Morimoto, Ed Nonnweiler, Sharbel Noujaim, Mitsuhiro Nozaki, Tim Nustad, Lloyd Ober, Satchi Panda, Kathy Panton, Brenda Peck, Pat Piacente, Joe Piel, Pat Potrykus, Sussan Pourjavid, Ted Rhyne, Bill Rohling, Tom Sabourin, Kazuo Sakamoto, Jack Schneider, Ray Schnoor, Patti Schubert, Said Seyed-Boloforosh, Toru Shimazaki, Jack Sleeter, Jon Snyder, Liliana Sprinceanu, Rob Steins, Jeff Strother, Kota Taguchi, Nim Tea, Tom Thomas, Venkat Venkataramani, Jim Voigt, Kirby Vosburgh, Hsifu Wang, Mike Washburn, and Renee Whitney. Their collaboration in and support of this work is deeply appreciated.

References

[1] J. F. Gelly and C. Maerfeld, "Properties for a 2D multiplexed array for acoustic imaging," *Proc. IEEE Ultrason. Symp.*, 1981, pp. 685–689.

[2] T. Kojima, "Matrix array transducer and flexible matrix arry (*sic*) transducer," *Proc. IEEE Ultrason. Symp.*, 1986, pp. 649–654.

[3] M. G. Maginness, J. D. Plummer, W. L. Beaver, and J. D. Meindl, "State-of-the-art in two-dimensional transducer array technology," *Med. Phys.*, vol. 3, pp. 312–318, 1976.

[4] M. Pappalardo, "Hybrid linear and matrix acoustic arrays," *Ultrasonics*, vol. 19, pp. 81–86, 1981.

[5] J. D. Plummer, R. G. Swartz, M. G. Maginness, J. R. Beaudouin, and J. D. Meindl, "Two-dimensional transmit/receive ceramic piezoelectric arrays: Construction and performance," *IEEE Trans. Sonics Ultrason.*, vol. 25, pp. 273–280, 1978.

[6] J. J. Rownd, E. L. Madsen, J. A. Zagzebski, and G. R. Fink, "Automated system for rapid ultrasound performance and QA testing in terms of detectability of low contrast focal lesions," *Ultrason. Imaging*, vol. 17, p. 60, 1995.

[7] D. Vilkomerson, J. Greenleaf, and V. Dutt, "Towards a resolution metric for medical ultrasonic imaging," *Proc. IEEE Ultrason. Symp.*, 1995, pp. 1405–1410.

[8] P. Tournois, S. Calisti, Y. Doisy, J. M. Bureau, and F. Bernard, "A 128∗4 channels 1.5D curved linear array for medical imaging," *Proc. IEEE Ultrason. Symp.*, 1995, pp. 1331–1335.

[9] G. R. Harris, "Review of transient field theory for a baffled planar piston," *J. Acoust. Soc. Amer.*, vol. 70, no. 1, pp. 10–20, 1981.

[10] ——, "Transient field of a baffled planar piston having an arbitrary vibration amplitude distribution," *J. Acoust. Soc. Amer.*, vol. 70, no. 1, pp. 186–204, 1981.

[11] B. Piwakowski and B. Delannoy, "Method for computing spatial pulse response: Time-domain approach," *J. Acoust. Soc. Amer.*, vol. 86, no. 6, pp. 2422–2432, 1989.

[12] H. Lasota, R. Salamon, and B. Delannoy, "Acoustic diffraction analysis by the impulse method: A line impulse response approach," *J. Acoust. Soc. Amer.*, vol. 76, pp. 280–290, 1984.

[13] G. S. Kino, *Acoustic Waves: Devices, Imaging and Analog Signal Processing*. Englewood Cliffs, NJ: Prentice-Hall, 1987.

[14] C. M. W. Daft, D. G. Wildes, L. J. Thomas, L. S. Smith, R. S. Lewandowski, W. M. Leue, K. W. Rigby, C. L. Chalek, and W. T. Hatfield, "A 1.5D transducer for medical ultrasound," *Proc. IEEE Ultrason. Symp.*, 1994, pp. 1491–1495.

[15] T. Shimazaki, M. Ando, and H. Tabei, "Ultrasound diagnosing device," U. S. Patent 5 083 568, Jan. 28 1992, assigned to Yokogawa Medical Systems, Ltd.

[16] D. G. Miller, "Ultrasonic transducer system," U. S. Patent 5 301 168, Apr. 5 1994, assigned to Hewlett-Packard Co.

[17] S. W. Flax and M. O'Donnell, "Phase aberration correction in medical ultrasound: Basic principles," *IEEE Trans. Ultrason., Ferroelect., Freq. Contr.*, vol. 35, pp. 758–767, 1988.

[18] C. Dorme and M. A. Fink, "Ultrasonic beam steering through inhomogeneous layers with a time reversal mirror," *IEEE Trans. Ultrason., Ferroelect., Freq. Contr.*, vol. 43, pp. 167–175, 1996.

[19] G. C. Ng, S. S. Worrell, P. D. Freiburger, and G. E. Trahey, "A comparative evaluation of several algorithms for phase aberration correction," *IEEE Trans. Ultrason., Ferroelect., Freq. Contr.*, vol. 41, pp. 631–643, 1994.

[20] P. C. Li and M. O'Donnell, "Phase aberration correction on two-dimensional conformal arrays," *IEEE Trans. Ultrason., Ferroelect., Freq. Contr.*, vol. 42, pp. 73–82, 1995.

[21] S. W. Smith, G. E. Trahey, and O. T. von Ramm, "Two dimensional arrays for medical ultrasound," *Ultrason. Imaging*, vol. 14, pp. 213–233, 1992.

[22] D. H. Turnbull and F. S. Foster, "Two-dimensional transducer arrays for medical ultrasound: Beamforming and imaging," in *New Developments in Ultrasonic Transducers and Transducer Systems*, F. L. Lizzi, Ed., *Proc. SPIE* 1733, pp. 202–215, 1992.

[23] R. E. Davidsen, J. A. Jensen, and S. W. Smith, "Two dimensional random arrays for real time volumetric imaging," *Ultrason. Imaging*, vol. 16, pp. 143–163, 1994.

[24] P. K. Weber, R. M. Schmitt, B. D. Tylkowski, and J. Steck, "Optimization of random sparse 2-D transducer arrays for 3-D electronic beam steering and focusing," *Proc. IEEE Ultrason. Symp.*, 1994, pp. 1503–1506.

[25] C. R. Cooly and B. S. Robinson, "Synthetic focus imaging using partial datasets," *Proc. IEEE Ultrason. Symp.*, 1994, pp. 1539–1542.

[26] G. R. Lockwood, P. C. Li, M. O'Donnell, and F. S. Foster, "Optimizing the radiation pattern of sparse periodic linear arrays," *IEEE Trans. Ultrason., Ferroelect., Freq. Contr.*, vol. 43, pp. 7–14, 1996.

[27] G. R. Lockwood and F. S. Foster, "Optimizing the radiation pattern of sparse periodic two dimensional arrays," *IEEE Trans. Ultrason., Ferroelect., Freq. Contr.*, vol. 43, pp. 15–19, 1996.

Douglas G. Wildes (M'85) received the A.B. degree in physics and mathematics from Dartmouth College, Hanover, NH, in 1978, and the M.Sc. and Ph.D. degrees in physics from Cornell University, Ithaca, NY, in 1982 and 1985, respectively.

He joined GE Corporate Research and Development in 1985, working initially on the development of a real-time system and signal analysis algorithms for detecting tool failures during the machining of aircraft engine parts. In 1991, he joined the Ultrasound Program, where he has worked on most aspects of phased-array transducer development. For the past several years, he has been project leader for development of multi-row transducers.

Dr. Wildes is a member of the American Physical Society and the IEEE.

Richard Y. Chiao (SM'85–M'90) was born in Taipei, Taiwan, in 1963. He received the B.S., M.S., and Ph.D. degrees in 1985, 1987, and 1990, respectively, from the Department of Electrical and Computer Engineering at the University of Illinois at Urbana/Champaign.

He joined GE Corporate Research and Development in 1990, where he initially worked on ultrasonic imaging for NDE. Since 1995, he has been with the medical ultrasound group at CRD working in the area of beamforming algorithms and architectures.

Chris M. W. Daft (M'88) was born in Dundee, Scotland, and received the B.A. and Ph.D. degrees from Oxford University, England, in 1984 and 1987, respectively.

From 1987 to 1990 he was with the Bioacoustics Research Laboratory of the Department of Electrical and Computer Engineering at the University of Illinois, as an Assistant Professor. He is currently with GE Corporate Research and Development, Schenectady, NY, in the ultrasound program. While at CRD, he has worked on many aspects of medical ultrasound imaging. Beamforming using VLSI chips has been one focus, as has design of color flow processors. As part of this, he initiated a loosely coupled multi-processor, bit-level simulation of GE's new ultrasound machines. The chips from this work now form the heart of GE's leadership ultrasound system. He has also investigated new types of transducers from a theoretical and experimental viewpoint. Current interests include the optimal detection of ultrasound data, low-cost approaches to beamforming, and transitioning of array design technology to the business.

Wayne Rigby (M'93) received the B.S. in physics from Yale University in 1979 and the Ph.D. in physics from Stanford University in 1986.

From 1986 to 1989 he was a postdoctoral scholar at Stanford University, working on a NASA space shuttle experiment. Since 1989 he has worked at GE Corporate Research and Development in Schenectady, NY. His interests include digital beamforming, especially adaptive beamforming for medical ultrasound imaging.

Dr. Rigby is a member of the IEEE and the American Physical Society.

L. Scott Smith (M'90) earned a B.S. from the University of Rochester, Rochester, NY, in 1972, and a Ph.D. in 1976 from the University of Pennsylvania, Philadelphia, PA, both in physics.

Since joining GE Corporate Research and Development in 1976, he has worked primarily on medical imaging. He has been cited for his contributions to phased array transducers, digital ultrasound imaging, and high field nuclear magnetic resonance imaging and spectroscopy. Recently he has also worked on transducers for pediatric cardiology.

A member of the American Physical Society and the IEEE, Dr. Smith is the author of over 25 papers and 20 patents on medical imaging.

Kai E. Thomenius (M'69) earned B.S., M.S. and Ph.D. degrees from Rutgers University, New Brunswick, NJ, in 1968, 1970, and 1978, respectively, all in electrical engineering.

After teaching at Rutgers and Stevens Institute of Technology, he has held positions of Project Engineer and Director of Research at Picker Ultrasound, Elscint, Interspec, and ATL. He is currently working on beamformer architectures and algorithms at GE Corporate Research and Development in Schenectady, NY. He has been involved with several aspects of ultrasound systems development including synthetic aperture arrays, Doppler processing, and the study of thermal bioeffects.

Dr. Thomenius is a Fellow of the American Institute of Ultrasound in Medicine, and a member of the IEEE, the American Society of Echocardiography, and the American Association of Physicists in Medicine.